Int J Adv Manuf Technol (2016) 82:1815–1821
DOI 10.1007/s00170-015-7458-7

ORIGINAL ARTICLE

Mechanism of material removal during orthogonal cutting of graphite/polymer composites

Zhenping Wan [1] · Dayong Yang [1] · Longsheng Lu [1] · Jing Wu [2] · Yong Tang [1]

Received: 2 December 2014 / Accepted: 17 June 2015 / Published online: 11 July 2015

Abstract With the engineering applications of graphite and its composites increasing, machining of graphite and its composites has attracted a great deal of attention. However, the cutting mechanisms of graphite and its composites are different from metals and other brittle materials because of specific crack initiation and propagation laws. This paper establishes a finite element model to calculate the effective stress field of the cutting zone during the orthogonal cutting of graphite/polymer composites. The crack initiation and propagation path in the cutting zone is determined by the smallest effective stress gradient at different cutting thicknesses and verified by edge-indentation experiments. Based on the crack initiation and propagation laws, a model of the graphite/polymer composites cutting process is proposed to understand the mechanism of material removal as well as machined surface formation. The cutting process of graphite/polymer composites can be divided into three stages: removal of large blocks, tiny blocks, and small blocks of graphite, which results in large, tiny, and small concavities, respectively, remaining on the machined surface. The cutting model is validated through machined surface morphology, cutting force, and chip morphology.

Keywords Graphite/polymer composites · Crack initiation and propagation · Cutting model · Machined surface morphology · Chip morphology

✉ Longsheng Lu
meluls@scut.edu.cn

[1] School of Mechanical and Automotive Engineering, South China University of Technology, Guangzhou 510640, China

[2] School of Urban Rail Transit, Guangdong Communication Polytechnic, Guangzhou 510650, China

1 Introduction

Graphite and its composites, which are superior in terms of lubricity, thermal and chemical resistance, thermal and electric conductivity, biocompatibility, and so on, have been used in various applications, such as motor brushes, electrodes of electrical discharge machines, pile cores, mechanical seals [1], bipolar plates of proton exchange membrane fuel cells [2] or direct methanol fuel cells [3], and biomedical implants [4]. High-purity graphite components have been adopted in semiconductor manufacturing processes such as ion implantation, plasma etching, and electron beam evaporation [5]. Therefore, the machining of graphite and its composites has received considerable attention. Schroeter et al. [6] performed graphite machinability tests and analyzed tool wear and surface quality generated in down- and up-milling. Zhou et al. [7] investigated the tool wear characteristics in the high-speed milling of graphite using a coated carbide micro endmill. Wang et al. [8] discussed the characteristics of tool wear and cutting forces when high-speed milling a graphite electrode. Cabral et al. [9] compared the cutting performance of diamond-coated tool inserts using hot filament chemical vapor deposition and time-modulated chemical vapor deposition. Cabral et al. [10] also investigated the impact of the surface roughness of diamond coatings on the cutting performance when dry machining of graphite. Almeida et al. [11] evaluated the cutting performance of micro- and nano-crystalline chemical vapor deposition diamond-coated silicon nitride ceramic tools in turning of a graphite electrode. To produce parts with the desired quality, the design of experiments methods [5], artificial neural networks [12], and grey relational analysis method [13] were applied to determine an optimal machining parameter setting when dry end-milling of high-purity graphite. Huo et al. [14] investigated the micro milling of fine-grained graphite using the design of experiments techniques.

Mijušković et al. [15] analyzed the tool deflection analytically and experimentally in the micro milling of graphite electrodes. These investigations concentrated on the machinability of graphite, tool wear characteristics, cutting performance of diamond-coated tool inserts, and optimization of cutting parameters. There have been few studies regarding the cutting mechanism of graphite. Masuda et al. [1] illustrated the chip formation process when turning the carbon phase and graphite phase. Wang et al. [8] and Zhou et al. [16] studied the characteristics of graphite chip formation by recording the graphite chip formation process at different depths of cut using a stereomicroscope. Therefore, the cutting mechanisms of graphite and its composites are not fully understood.

Cracks occur and propagate easily during graphite machining since graphite is a brittle material. The initiation and propagation of cracks at the cutting zone result in chippings by scooping out the workpiece material in a large amount. Hence, the machining mechanisms of graphite and its composites differ from metals and other brittle materials because of their specific crack initiation and propagation laws. Therefore, it is much needed to conduct research on the mechanism of material removal to gain a better understanding of the machining processes of graphite and to improve the machined surface qualities.

The purpose of this study is to understand the mechanism of material removal and machined surface formation during the orthogonal cutting of graphite/polymer composites. The crack initiation and propagation path are predicted based on the smallest effective stress gradient direction of the effective stress field in the cutting zone and are verified by edge-indentation experiments. Based on the crack initiation and propagation laws, a model of the graphite/polymer composites cutting process is proposed to disclose the mechanism of material removal and machined surface formation. Finally, the model is validated through machined surface morphology, cutting force, and chip morphology.

2 Crack initiation and propagation laws

The primary mechanism of material removal is crack initiation and propagation which is decided by the effective stress field of the cutting zone. Hence, an analysis of the effective stress field of the cutting zone is helpful for understanding the material removal mechanism of graphite/polymer composites cutting.

2.1 Finite element modeling for stress field analysis

The graphite/polymer composites used in this study are some types of coke, natural graphite, which are ground, sieved, and added to a binder (polymer). The paste is homogenized and placed in a mold and then sufficiently compacted.

Table 1 Mechanical properties of the graphite/polymer composites

Properties	Values
Density	1.9 g/cm^3
Hardness	75 HS
Tensile strength	17.3 MPa
Compressive strength	107.2 MPa
Elastic modulus	15.9 GPa

Subsequently, the material is baked slowly at high temperature. This type of graphite/polymer composite has been widely applied to bipolar plates of proton exchange membrane fuel cells and direct methanol fuel cells. The mechanical properties are listed in Table 1. The stress–strain relationship of the graphite/polymer composite can be shown as [17]:

$$\varepsilon = A\sigma + B\sigma^2 \tag{1}$$

where ε and σ denote strain and stress, respectively. A and B are constants. $A=1/E$, and E is the elastic modulus; B is 0.946×10^{-6} MPa^{-2}, as determined by uniaxial tensile tests.

ANSYS explicit dynamics is used to calculating the effective stress field of the cutting zone. The generalized boundary conditions are shown in Fig. 1. The size of the workpiece is 50 mm×10 mm×25 mm, and the bottom of the workpiece is grounded, whereas the tool is given a constant velocity of 6 m/min and all of the other translational and rotational degrees of freedom are constrained. The cutting thickness is 0.5, 1, and 2 mm, respectively. Therefore, the cutting operation is orthogonal cutting and can be simplified as a plane strain model. Note that no significant temperature rise has been observed experimentally due to the slow cutting velocity. Hence, the dependence of the properties on temperature has not been considered. In this model, a classical Coulomb friction law is assumed to model the tool-workpiece contact zone. The friction coefficient is defined as $\mu=F_t/F_n$, where F_t is the rake face tangential force and F_n is the rake face perpendicular force. A value of $\mu=0.5$ is assumed, which has been selected based on the rake face friction coefficient identification results. A very dense mesh is defined in the area of the cutting zone and relatively large elements for the rest of the

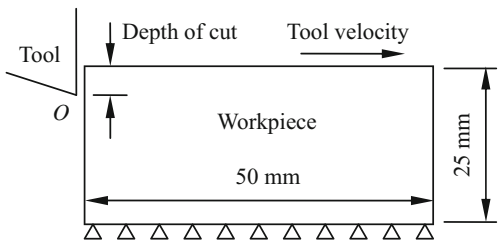

Fig. 1 Cutting geometry and boundary conditions

workpiece, as shown in Fig. 2. A total of 28,300 quadrilateral meshes are used for modeling the workpiece. The tool is considered as a rigid body with rake angle of 0° and clearance angle of 10°.

2.2 Effective stress field and crack propagation path

In the three-dimensional stress states, according to Paul and Mirandy's theory [18], if $(\sigma_{III}/\sigma_b)<(1-N_1^2)$, then the fracture criterion is

$$\sigma_{eff} = \frac{N_1(\sigma_I + \sigma_{III}) + 2\sqrt{N_1^2\sigma_I\sigma_{III} + (\sigma_I - \sigma_{III})^2}}{N_1(4 - N_1^2)} \quad (2)$$

where σ_{eff} is the effective stress, and σ_I and σ_{III} are the maximum principal stress and minimum principal stress, respectively. N_1 is calculated by

$$N_1 = \sqrt{2 + \frac{\sigma_c}{\sigma_b} - 2\sqrt{1 + \frac{\sigma_c}{\sigma_b}}} \quad (3)$$

where σ_c and σ_b stand for the compressive strength and tensile strength, respectively. If $\sigma_{III}/\sigma_b \geq (1-N_1^2)$, the fracture criterion is expressed as

$$\sigma_{eff} = \sigma_I. \quad (4)$$

When the tool just enters the workpiece, the effective stress fields of the cutting zone at rake angle of 0° and cutting thickness of 0.5, 1, and 2 mm are shown in Fig. 3 where the capital A, B, C, and so on stand for the effective stress isoline and the point *O* stands for the tool apex. In Fig. 3, the effective stresses at the tool apex are maximal and have just reached the tensile strength of the graphite/polymer composites. The effective stresses decrease gradually away from the tool apex at the cutting zone. As the tools advance, cracks will occur at the tool apex. Subsequently, the initiated cracks progress along the smallest effective stress gradient direction which is

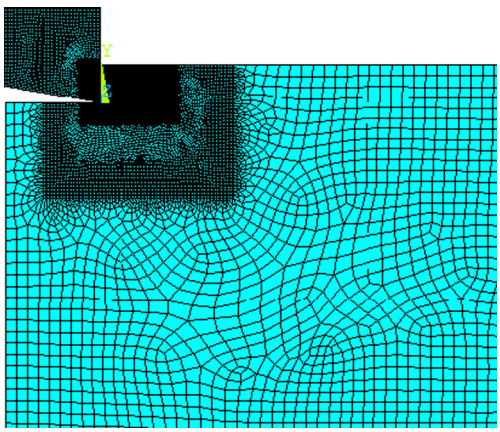

Fig. 2 Finite element mesh

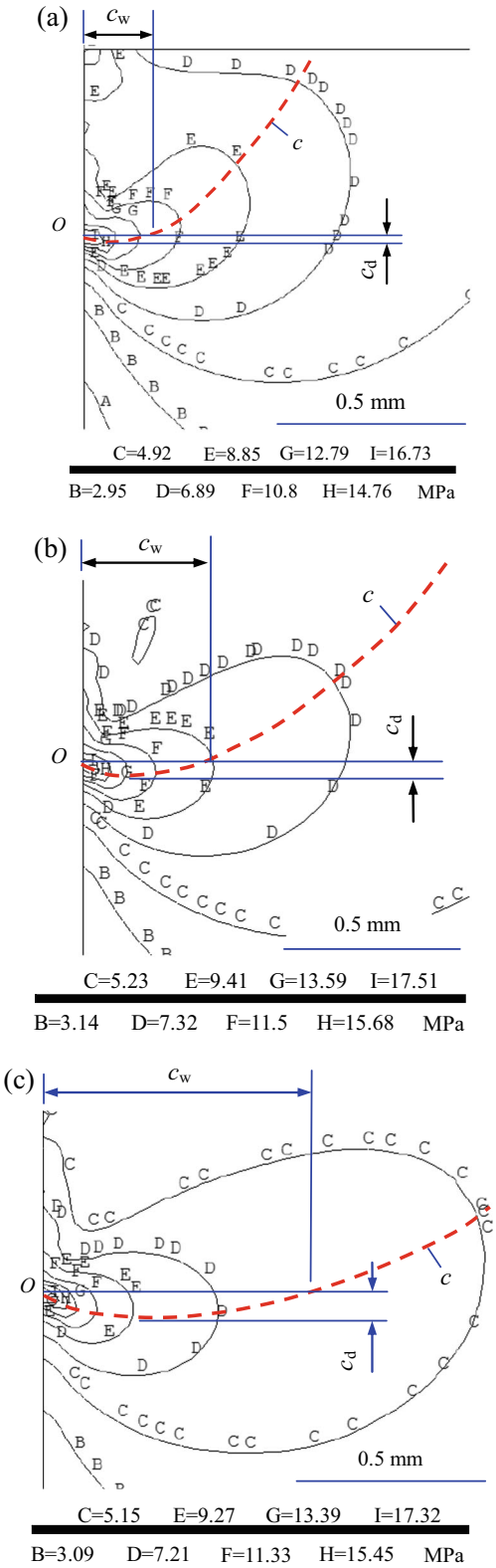

Fig. 3 Effective stress field and crack propagation path at 0° rake angle and cutting thicknesses of **a** 0.5, **b** 1, and **c** 2 mm

indicated by curve c. Thus, the curve c denotes the propagation path of crack. Therefore, the crack c initiates at the apex of tool and propagates downward; then it spreads upward gradually and finally reaches the surface of workpiece. The propagation path of the crack is approximately arc shaped. Therefore, a block of the workpiece material surrounded by the crack c is removed as the tool proceeds and a concavity remains on the machined surface. In Fig. 3, c_w and c_d indicate the width and depth of the concavities, respectively. It can be observed that c_w and c_d increase with cutting thickness increasing. In other words, the larger the cutting thickness, the larger the concavities formed on the machined surface.

2.3 Verification of crack initiation and propagation path

The analytical results from the above finite element model should be validated with experimental results. Edge indentation experiments are conducted to verify the predication of the crack initiation and propagation path. A schematic drawing of edge indentation is presented in Fig. 4, where P indicates the load imposed on the indenter and h_D denotes the indentation thickness. The dimensions of the specimen are 65×40×5 mm. The indentation surface of the specimen is polished so that no cracks can be observed. The material of the indenter is high-speed steel and the included angle φ is 75°. The indenter can adjust by itself so that well distribution of pressure is achieved on the indentation surface.

From Fig. 4, the edge indentation is similar to the orthogonal cutting if the indenter is deemed as cutting tool and h_D is equivalent to cutting thickness. For example, the indenter corresponds to the cutting tool with rake angle of 15° and clearance angle of 0° when φ is 75°. Therefore, the laws of crack initiation and propagation from the edge indentation experiments can be applied to verify the analytic results from the finite element mode.

Figure 5 presents the crack initiation and propagation path of edge-indentation at indentation thicknesses of 0.5, 1, 1.5, and 2 mm when φ is 75°. The cracks initiate at the apex of the tool and propagate down- and forward; then they gradually spread upward to the specimen surface. The propagation path of the cracks is like a segment of a circular arc. By comparing Figs. 3 and 5, the predicted crack propagation paths are in good agreement with the experimental results. From Fig. 5, a block of graphite surrounded by a crack is removed and a concavity remains on the surface. The width and depth of the concavities that remain on the specimen surface show strong dependence on the indentation thickness, as shown in Fig. 6. The width and depth of the concavities increase with indentation thickness increasing linearly and the width rises with a larger slope, which is also in accordance with the predicted results.

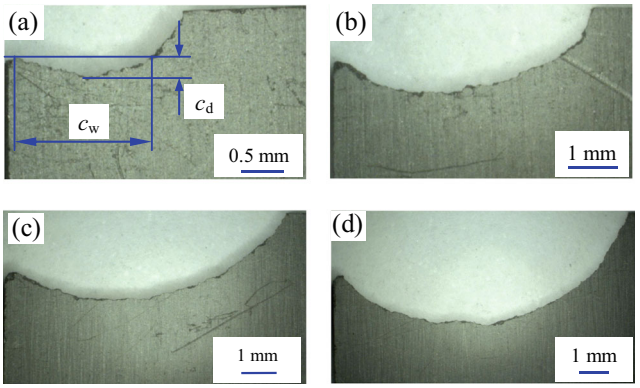

Fig. 5 Crack initiation and propagation path of edge indentation (φ= 75°) **a** h_D=0.5 mm, **b** h_D=1 mm, **c** h_D=1.5 mm, and **d** h_D=2 mm

3 Model of the graphite/polymer composites cutting process

Based on the previous analysis, a crack occurs at the apex of the tool when the tool enters into the workpiece. The crack spreads downward to the cutting velocity and then gradually grows upward to the workpiece surface as the tool advances. The propagation path can be considered as an arc-shaped segment. Hence, a block of graphite encompassed by a crack is removed and a concavity remains on the machined surface. Furthermore, it can be inferred that a large block of graphite will be removed and that a concavity with large width and

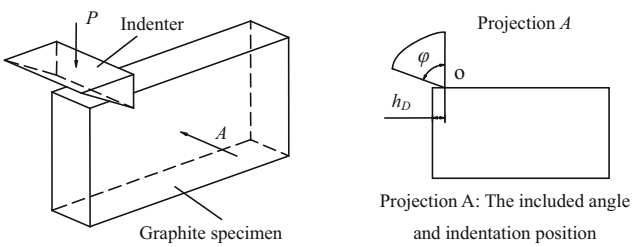

Fig. 4 Schematic drawing of edge indentation on a graphite/polymer specimen

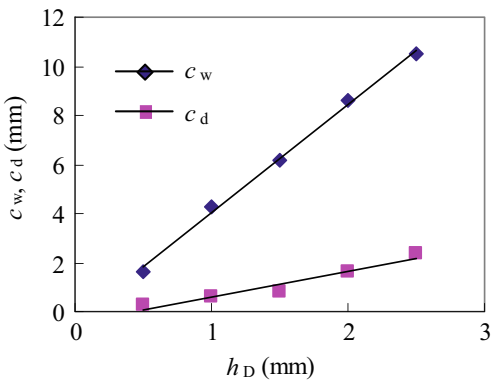

Fig. 6 Width and depth of concavities at different indentation thicknesses

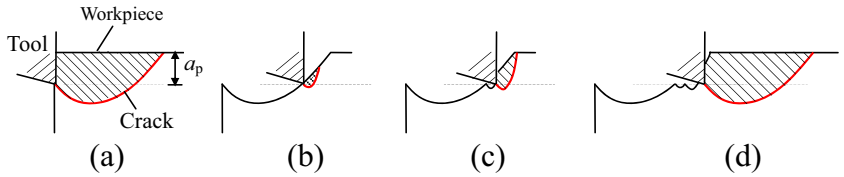

Fig. 7 Model of the graphite/polymer composites cutting process. **a** Removal of a large block of graphite, **b** removal of a tiny block of graphite, **c** removal of a small block of graphite, and **d** next cycle

depth will form on the machined surface if cutting thickness is large. When the cutting thickness is thin, a small block of graphite surrounded by a crack will be removed and, correspondingly, a small concavity will form on the machined surface. Based on the analysis of the effective stress field and crack initiation and propagation laws, a model of the graphite/polymer composites cutting process is proposed to understand the mechanism of material removal and machined surface formation. The graphite/polymer composites cutting process can be divided into three stages: removal of a large block of graphite and then removal of a tiny block of graphite followed by removal of a small block of graphite.

(1) Removal of a large block of graphite. When the tool enters the workpiece, a stress field forms in the front of the rake face. When the maximum effective stress reaches a critical value, a crack initiates at the tool apex and grows outward and downward, and then it propagates toward the workpiece surface. Accordingly, a large block of graphite surrounded by the crack is removed and a large concavity forms on the machined surface, as shown in Fig. 7a.

(2) Removal of a tiny block of graphite. Once a large concavity forms on the machined surface, the tool passes through the concavity and nothing is cut. Then, the cutting thickness gradually increases from zero once the tool cuts into the workpiece again. At this stage, the crack hardly spreads downward because of the tiny cutting thickness. Therefore, only tiny blocks of graphite are removed and the machined surface with high integrity is obtained, as shown in Fig. 7b.

(3) Removal of a small block of graphite. As the tool continues forward, the cutting thickness increases gradually, but is still small. The crack spreads outward and downward slightly. Thus, a small block of graphite surrounded by the crack is removed and a small concavity forms on the machined surface, as shown in Fig. 7c. At this stage, the processes maybe occur repeatedly. It gives rise to many small concavities on the machined surface. As the cutting proceeds, the cutting thickness increases continually until it is close to the initial cutting thickness. Subsequently, the whole process begins over again as shown in Fig. 7d.

4 Model validation

Based on the model of the graphite/polymer composites cutting process described above, the machined surface is composed of periodically repeating large, tiny, and small concavities if the cutting thickness is large. Furthermore, if the cutting thickness is small enough, only tiny blocks of graphite are removed and tiny concavities or even no concavities form on the machined surface because cracks generated in the cutting zone barely spread toward the machined surface. These steps can be validated by the machined surface morphology, cutting force, and chip morphology.

4.1 Experimental setup

Dry orthogonal cutting experiments are performed on a planer BC6063B. In order to obtain typical machined surface composed of large, tiny, and small concavities, a cutting tool with rake angle of 20° is used to machining the graphite/polymer workpiece with width of 5 mm. The cutting tool with clearance angle of 10° is made of high-speed steel. It is suggested from mass experiments that the cutting speed is almost without influence upon machined surface formation. Additionally, from reference [8], the cutting speed has little influence on the cutting forces in the milling of graphite electrode. Therefore, the cutting speed is set to a low constant velocity of 6 m/min. The Kistler dynamometer and its mating data acquisition system are used to measure and record the cutting force. The

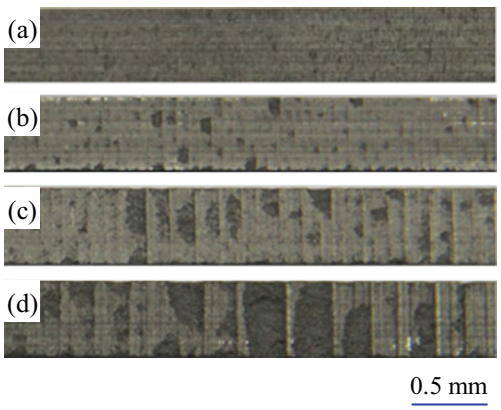

Fig. 8 Machined surface morphologies at rake angle of 20°, cutting speed of 6 m/min, and cutting thicknesses of **a** 0.2, **b** 0.4, **c** 0.6, and **d** 0.8 mm

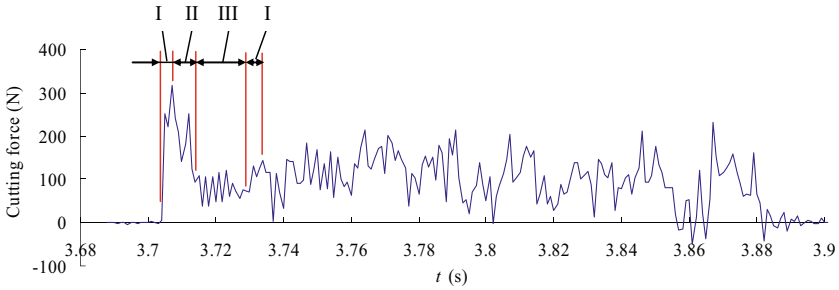

Fig. 9 Dynamic horizontal cutting forces (γ_o=0°, a_p= 0.4 mm, v=6 m/min)

Keyence microscope (VHX-1000E) is used to observe the chip morphologies.

4.2 Model validation in terms of machined surface morphology

Figure 8 presents the machined surface morphologies obtained at cutting thicknesses of 0.2, 0.4, 0.6, and 0.8 mm. When the cutting thickness is 0.2 mm, the machined surface is composed of very tiny concavities, as shown in Fig. 8a, since the cutting thickness is small. It can be seen from Fig. 8b–d that the machined surface is composed of large concavities followed by tiny or small concavities; then, the cycle begins over again when the cutting thickness is greater than or equal to 0.4 mm. This conforms to the model of the graphite/polymer composites cutting process shown in Fig. 7. In addition, the model captures the effect of increase in the cutting thickness on the machined surface: The greater the cutting thickness, the larger are the concavities. Therefore, the model of the graphite/polymer composites cutting process is validated by the machined surface morphologies.

4.3 Model validation in terms of cutting force

The dynamic horizontal cutting forces are presented in Fig. 9, in which the rake angle of the tool is 0°, the cutting thickness is 0.4 mm and the cutting speed is 6 m/min. It can be observed from Fig. 9 that the cutting forces fluctuate greatly with high frequency. The fluctuation of the cutting forces seems to be stochastic, but in fact, it is cyclical and can be associated with the model of the cutting process. When the tool cuts into the workpiece, the cutting forces increase dramatically, as indicated by stage I in Fig. 9. As the tool moves forward, the crack initiates and propagates in the cutting zone. Crack initiation and propagation result in cutting forces decreasing, as denoted by stage II. When the block surrounded by the crack is removed, a concavity forms on the machined surface. When this occurs, the cutting force is minimal because the tool is crossing the concavity and corresponds with stage III. After the tool pass through the concavity, the tool cuts into the workpiece again. At that moment, the cutting force increases and the next cycle occurs, although the subsequent cycles are not so typical. Therefore, the dynamic cutting forces also validate the model of the graphite/polymer composites cutting process.

4.4 Model validation in terms of chip morphology

Figure 10 shows the chip morphologies obtained at cutting thicknesses of 0.2 and 0.4 mm. The fragmented chips form because of crack initiation and propagation, as predicted by the model, and also, the chips consist of large, small, and tiny blocks. Therefore, it can be inferred that the surface material of the workpiece is removed in large, small, and tiny blocks, which validates the model of the graphite/polymer composites cutting process further. Moreover, the model captures the effects of cutting thickness increasing on material removal and machined surface formation because a larger the cutting thickness results in larger chip blocks.

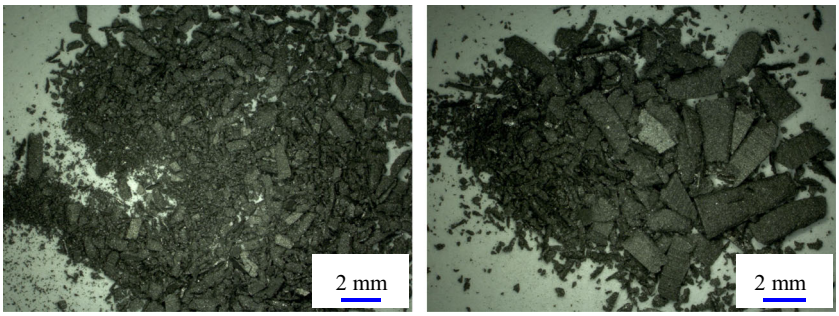

Fig. 10 Comparison of chip morphologies at rake angle of 20° and different cutting thicknesses: **a** 0.2 and **b** 0.4 mm

5 Conclusions

The current work focuses on the mechanisms of material removal and machined surface formation, which helps enhance the understanding of the fundamental processes of graphite/polymer composites cutting.

(1) The graphite/polymer cutting process is characterized by crack initiation and propagation. A crack initiates at the apex of the tool and propagates downward and outward; then, it spreads upward gradually until reaching the workpiece surface. The crack propagation path is arc shaped. Crack initiation and propagation result in the formation of concavities on the machined surface. The depth and width of concavities increase as the cutting thickness increases.

(2) A model of the graphite/polymer composites cutting process is proposed based on crack propagation laws. The graphite/polymer composites cutting process can be divided into three stages: removal of a large block of graphite and then removal of a tiny block of graphite followed by removal of a small block of graphite.

(3) The machined surface is composed of large concavities followed by tiny or small concavities and then the cycle repeats. The chips consist of large, small, and tiny blocks of graphite. The machined surface morphologies, cutting forces, and chip morphologies validate the model of the graphite/polymer composites cutting process.

Acknowledgments This research is based upon the work supported by the National Natural Science Foundation of China under Grant no. 51075155.

References

1. Masuda M, Kuroshima YK, Chujo Y (1996) The machinability of sintered carbons based on the correlation between tool wear rate and physical and mechanical properties. Wear 195:178–185
2. Suherman H, Sahari J, Sulong AB (2013) Effect of small-sized conductive filler on the properties of an epoxy composite for a bipolar plate in a PEMFC. Ceram Int 39:7159–7166
3. Stuebler N, Hickmann T, Ziegmann G (2013) Effect of methanol absorption on properties of polymer composite bipolar plates for direct methanol fuel cells. J Power Sources 229:223–228
4. Starý V, BačákováL HJ, Chmelík V (2003) Bio-compatibility of the surface layer of pyrolytic graphite. Thin Solid Films 433:191–198
5. Yang YK, Chuang MT, Lin SS (2009) Optimization of dry machining parameters for high-purity graphite in end milling process via design of experiments methods. J Mater Process Technol 209: 4395–4400
6. Schroeter RB, Kratochvil R, Gomes JD (2006) High-speed finishing milling of industrial graphite electrodes. J Mater Process Technol 179:128–132
7. Zhou L, Wang CY, Qin Z (2009) Tool wear characteristics in high-speed milling of graphite using a coated carbide micro endmill. Proc Inst Mech Eng B J Eng 223:267–277
8. Wang CY, Zhou L, Fu H, Hu ZL (2007) High speed milling of graphite electrode with endmill of small diameter. Chin J Mech Eng En 20:27–31
9. Cabral G, Reis P, Polini R, Titus E, Ali N, Davim JP, Grácio J (2006) Cutting performance of time-modulated chemical vapour deposited diamond coated tool inserts during machining graphite. Diam Relat Mater 15:1753–1758
10. Cabral G, Reis P, Titus E, Madaleno JC, Davim JP, Grácio J, Ahmed W, Jackson MJ (2008) Impact of surface roughness of diamond coatings on the cutting performance when dry machining of graphite. Int J Manuf Technol Manag 15:121–152
11. Almeida FA, Sacramento J, Oliveira FJ, Silva RF (2008) Micro- and nano-crystalline CVD diamond coated tools in the turning of EDM graphite. Surf Coat Technol 203:271–276
12. Shie JR (2006) Optimization of dry machining parameters for high purity graphite in end-milling process by artificial neural networks: a case study. Mater Manuf Process 21:838–845
13. Yang YK, Shie JR, Huang CH (2006) Optimization of dry machining parameters for high-purity graphite in end-milling process. Mater Manuf Process 21:832–837
14. Huo DH, Lin C, Dalgarno K (2014) An experimental investigation on micro machining of fine-grained graphite. Int J Adv Manuf Technol 72:943–953
15. Mijušković G, Krajnik P, Kopač J (2015) Analysis of tool deflection in micro milling of graphite electrodes. Int J Adv Manuf Technol 76:209–217
16. Zhou L, Wang CY, Qin Z (2009) Investigation of chip formation characteristics in orthogonal cutting of graphite. Mater Manuf Process 24:1365–1372
17. Jenkins GM (1962) Analysis of the stress–strain relationships in reactor grade graphite. Br J Appl Phys 13:30–32
18. Paul B, Mirandy L (1976) Improved fracture criterion for three-dimensional stress states. J Eng Mater Technol ASME 98:159–163